

# An Improved Global Model for Air-Sea Exchange of Mercury: High Concentrations over the North Atlantic

ANNE L. SOERENSEN,<sup>†,‡</sup>  
 ELSIE M. SUNDERLAND,<sup>\*,‡,§</sup>  
 CHRISTOPHER D. HOLMES,<sup>‡</sup>  
 DANIEL J. JACOB,<sup>‡</sup>  
 ROBERT M. YANTOSCA,<sup>‡</sup> HENRIK SKOV,<sup>†</sup>  
 JESPER H. CHRISTENSEN,<sup>†</sup>  
 SARAH A. STRODE,<sup>||</sup> AND  
 ROBERT P. MASON<sup>±</sup>

National Environmental Research Institute, Aarhus University, Frederiksborgvej 399, DK-4000 Roskilde, Denmark, School of Engineering and Applied Sciences and Department of Earth and Planetary Sciences, Harvard University, Cambridge Massachusetts 02138, United States, Department of Environmental Health, Harvard University School of Public Health, Boston Massachusetts 02115, United States, Department of Atmospheric Sciences, University of Washington, Seattle, Washington 98195, United States, and Department of Marine Sciences, University of Connecticut, 1080 Shennecossett Road, Groton, Connecticut, 0634, United States

Received June 15, 2010. Revised manuscript received October 1, 2010. Accepted October 7, 2010.

We develop an improved treatment of the surface ocean in the GEOS-Chem global 3-D biogeochemical model for mercury (Hg). We replace the globally uniform subsurface ocean Hg concentrations used in the original model with basin-specific values based on measurements. Updated chemical mechanisms for Hg<sup>0</sup>/Hg<sup>II</sup> redox reactions in the surface ocean include both photochemical and biological processes, and we improved the parametrization of particle-associated Hg scavenging. Modeled aqueous Hg concentrations are consistent with limited surface water observations. Results more accurately reproduce high-observed MBL concentrations over the North Atlantic (NA) and the associated seasonal trends. High seasonal evasion in the NA is driven by inputs from Hg enriched subsurface waters through entrainment and Ekman pumping. Globally, subsurface waters account for 40% of Hg inputs to the ocean mixed layer, and 60% is from atmospheric deposition. Although globally the ocean is a net sink for 3.8 Mmol Hg y<sup>-1</sup>, the NA is a net source to the atmosphere, potentially due to enrichment of subsurface waters with legacy Hg from historical anthropogenic sources.

## Introduction

Anthropogenic mercury (Hg) sources have enriched atmospheric Hg deposition globally by at least a factor of 3 (1).

Atmospheric Hg is predominantly the gaseous elemental form (Hg<sup>0</sup>), and is oxidized to Hg<sup>II</sup>, which is then rapidly deposited. It is estimated that more than 80% of the Hg deposited to oceans is reemitted to the atmosphere as Hg<sup>0</sup>, driving the cycle of Hg through biogeochemical reservoirs (2). Aqueous reduction of divalent inorganic mercury (Hg<sup>II</sup>) and subsequent loss of Hg<sup>0</sup> reduces the potentially bioavailable Hg<sup>II</sup> pool that may be converted to monomethylmercury, the most toxic species that poses health risks to fish consuming populations and wildlife (3).

Previous efforts to model Hg air–sea exchange (2) and atmospheric transport (4–6) have been unable to reproduce high atmospheric concentrations observed in the Northern Hemisphere marine boundary layer (MBL) during ocean cruises (7–9). We hypothesize that this results from subsurface seawater Hg enrichment, reflecting the legacy of past anthropogenic inputs and controlling Northern Hemisphere MBL concentrations. Previous research comparing preindustrial and contemporary Hg budgets for different ocean basins indicates that anthropogenic enrichment of Hg reservoirs in the Atlantic Ocean and Mediterranean Sea is >50% (3). Other regions such as deep waters of the Pacific Ocean have seen negligible anthropogenic impacts while Hg concentrations in intermediate waters of the North Pacific (NP) appear to be increasing (10). These gradients in subsurface Hg across ocean regions (11, 12) have not been represented in models simulating atmospheric Hg. Here we investigate the potential effects of legacy anthropogenic Hg accumulation on oceanic air–sea exchange in the GEOS-Chem global model (1) by including the effects of variability in subsurface ocean concentrations in our simulation.

Most marine surface waters are supersaturated in Hg<sup>0</sup> (13, 14). A combination of biologically mediated (15–17) and photochemical (14, 18, 19) processes reduce atmospherically deposited Hg<sup>II</sup> in the water column to Hg<sup>0</sup>. Field and laboratory studies suggest that photolytic processes drive most Hg<sup>II</sup> reduction in surface waters but biotic reduction is also significant (16, 17, 19) and that aqueous Hg<sup>0</sup> oxidation involves reaction with photochemically produced OH<sup>•</sup> (17, 20). Oxidation rates appear to be enhanced in marine waters relative to freshwater (21, 22), possibly due the reaction of halides like Cl<sup>-</sup> and Br<sup>-</sup> with OH<sup>•</sup> to produce aqueous halogen radicals (23) or through the formation of stable Hg<sup>II</sup> complexes that decrease reduction rates (resulting in greater net oxidation) (17).

The original slab-ocean model in GEOS-Chem (2) represents oceanic Hg cycling in a simplified manner using three rate coefficients that describe net reduction of atmospherically deposited Hg<sup>II</sup>, conversion of Hg<sup>II</sup> to nonreactive particulate Hg (Hg<sup>p</sup>), and sinking of Hg<sup>p</sup>. Each rate coefficient is adjusted to match observations. Here we update the chemical mechanisms for surface ocean Hg reactions to include both photochemical and dark Hg<sup>0</sup> oxidation, and both photolytic and biotic Hg<sup>II</sup> reduction. We also model effects of light attenuation on redox reactions, Hg<sup>II</sup> sorption to particles, and Hg<sup>p</sup> removal from the surface layer based on export of organic carbon (24). We use the new model to investigate spatial and seasonal trends in oceanic Hg<sup>0</sup> evasion and the resulting Hg concentrations in the MBL.

## Materials and Methods

**General Model Description.** GEOS-Chem, a global scale chemical transport model (CTM), was adapted for atmospheric and oceanic Hg cycling by Selin et al. (5) and Strode et al. (2). We use the most recent version of Holmes et al. (25), including Br atoms as the main atmospheric oxidant

\* Corresponding author phone: +1-617-384-8832; e-mail: esunder@hsph.harvard.edu.

<sup>†</sup> Aarhus University.

<sup>‡</sup> Harvard University.

<sup>§</sup> Harvard University School of Public Health.

<sup>||</sup> University of Washington.

<sup>±</sup> University of Connecticut.

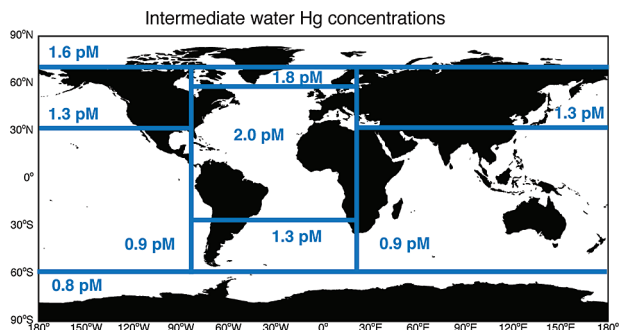


**FIGURE 1.** Subsurface ocean concentrations of inorganic Hg based on observations compiled by Sunderland and Mason (24), with recent measurement updates (10, 34).

for  $\text{Hg}^0$ . The model includes a 3-D atmospheric simulation (5), a 2-D surface-slab ocean simulation, and a 2-D dynamic terrestrial reservoir (1). We run simulations at  $4^\circ \times 5^\circ$  horizontal resolution with assimilated meteorological data for 2004–2008 from the NASA Goddard Earth Observing System (GEOS-5). Horizontal resolution of the surface ocean model is the same as the atmospheric model and the vertical depth varies depending on the monthly mixed layer depth (MLD) of the ocean (26). Three inorganic mercury forms are tracked by both the atmospheric and surface ocean simulations:  $\text{Hg}^{\text{II}}$ ,  $\text{Hg}^0$ , and  $\text{Hg}^{\text{P}}$ .

Atmospheric  $\text{Hg}^{\text{II}}$  and  $\text{Hg}^{\text{P}}$  enter the surface ocean through wet and dry deposition. Anthropogenic Hg emissions are from the GEIA inventory for the year 2000 (27), adjusted for recent changes based on projections by Streets et al. (28). We reduced emissions from geogenic sources by 50% relative to those in Selin et al. (1) for consistency with recent global estimates for natural emissions (29). The model is spun-up to steady state for preindustrial conditions to equilibrate the 2-D terrestrial model and then updated to present-day by including anthropogenic emissions and increasing the terrestrial concentrations, following the procedure described by Selin et al. (1). The present-day simulation is then conducted for 5 years to equilibrate the surface ocean and the stratosphere. We use year 2008 for analysis.

#### Exchange with the Atmosphere and Subsurface Waters.

Air–sea fluxes of  $\text{Hg}^0$  are modeled using the parametrization of Nightingale et al. (30), the Henry's law coefficient for  $\text{Hg}^0$  (31), a temperature-corrected Schmidt number for  $\text{CO}_2$  (32), and the Wilke–Chang method for estimating a temperature and salinity-corrected  $\text{Hg}^0$  diffusivity in different ocean regions (33) (see Supporting Information (SI) Table S4).

We retain vertical exchanges between the surface ocean and intermediate waters through entrainment/detrainment

of the mixed layer and Ekman (wind-driven) pumping included in the original GEOS-Chem slab ocean model (2). Deepening of the surface ocean mixed layer (26) results in entrainment of Hg from intermediate waters and seasonal surface stratification results in detrainment.

The original GEOS-Chem slab ocean model (2) assumed a globally uniform subsurface ocean Hg concentration. We updated this (Figure 1) using observations compiled by Sunderland and Mason (24), and new data for the NP (10) and Arctic (34) Oceans. The model presently neglects lateral transport in surface currents and the vertical diffusion flux, which was a small constant (nonphysical) value in the Strode et al. (2) model. Both of these simplifications are areas for future model development.

**Surface Ocean Redox Reactions.** Our model incorporates separate terms for photolytic and biotic reduction, and photochemical and dark oxidation (Figure 2). We base the reducible fraction of the dissolved  $\text{Hg}^{\text{II}}$  pool on estimates from freshwater systems (35) and data indicating that stable chloride complexes abundant at high salinities are more resistant to reduction processes (17, 36). Reported ranges for the reducible pool from the above studies vary between approximately 40% and 60% of total  $\text{Hg}^{\text{II}}$  and we implement a value of 40% to best match the observational constraints provided by specciated surface ocean and atmospheric Hg concentrations (Figures 3 and 4). Re-equilibration of all reactive and nonreactive pools and Hg speciation occurs at each time step (60 min) in the model simulation.

Measured biotic Hg reduction rate coefficients in dark seawater incubation experiments range from  $3.5 \times 10^{-7} \text{ s}^{-1}$  (37) to  $8.3 \times 10^{-5} \text{ s}^{-1}$  (18). These experiments assume instantaneous equilibration of any added Hg to mimic Hg speciation under natural conditions (i.e., the rate coefficients apply only to the reducible  $\text{Hg}^{\text{II}}$  fraction). Many studies report relationships between biotic reduction rate coefficients in natural waters and factors such as productivity, particulate matter and bacterial activity (17, 37, 38). A variety of rate coefficient data for  $\text{Hg}^{\text{II}}$  photoreduction are also available (16, 19, 21, 22, 39). While these data provide guidance, most cannot be implemented directly in the model because they reflect net  $\text{Hg}^{\text{II}}$  reduction rate coefficients, are for unfiltered waters (do not isolate photoreduction and biotic reduction), and/or do not report radiation intensities.

We therefore used dual isotope addition data from Whalin et al. (17), who measured simultaneous photo-oxidation ( $k_{\text{OX1}}$ ), photoreduction ( $k_{\text{RED1}}$ ), and biotic reduction ( $k_{\text{RED2}}$ ) rate coefficients ( $\text{s}^{-1}$ ) in Chesapeake Bay seawater. By least-squares fit to the Whalin et al. (17) data, we derived linear relationships between total shortwave solar radiation ( $R$ ,  $W$

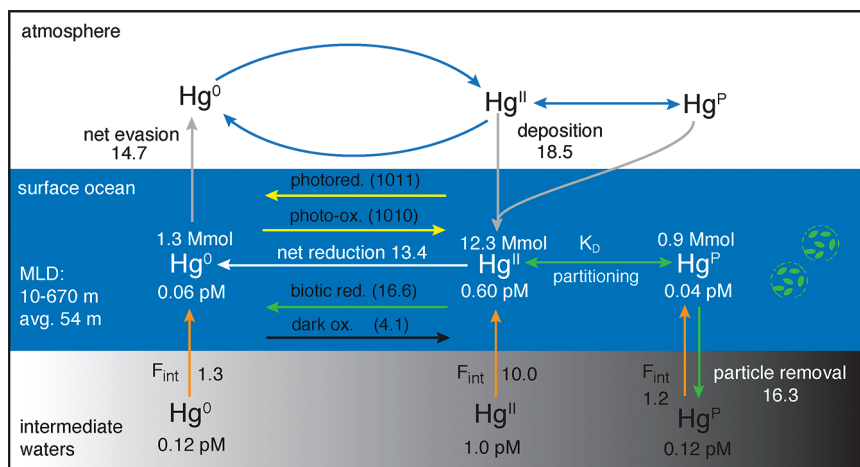


**FIGURE 2.** GEOS-Chem global budget of Hg in the surface ocean. Units are  $\text{Mmol y}^{-1}$  unless noted.  $F_{\text{int}}$  denotes net fluxes from intermediate waters through entrainment/detrainment of the mixed layer and Ekman pumping. MLD denotes mixing layer depth.

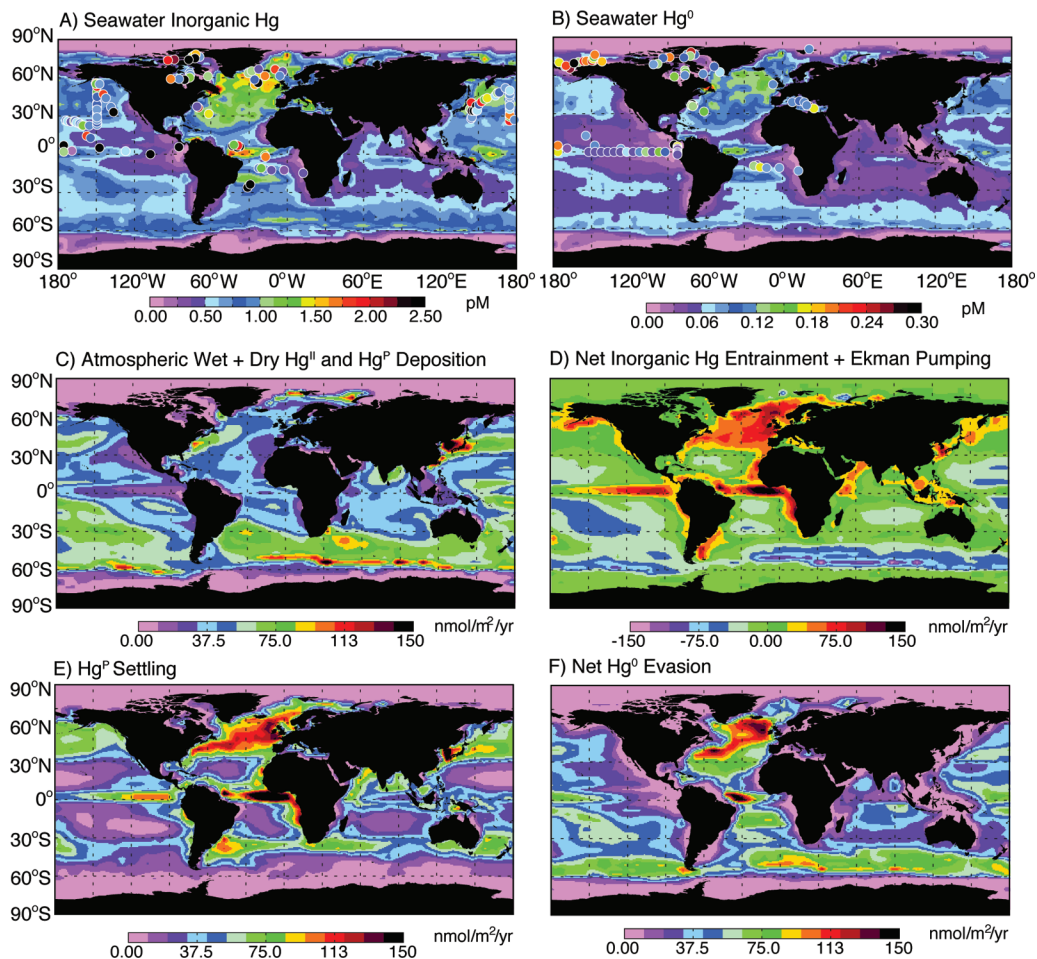


**FIGURE 3.** Global distribution of Hg concentrations and fluxes in the surface ocean. Fluxes and concentrations are annual mean values from the GEOS-Chem model simulation. Observed concentrations of total inorganic Hg and Hg<sup>0</sup> are shown as circles and include data from the Atlantic (14, 45, 52, 53); Pacific (10, 12, 44, 54); Arctic (13, 34). We omitted outliers in Hg<sup>0</sup> observations from two cruises in the Atlantic Ocean in the 1990s due to an apparent contamination problem (14, 45).

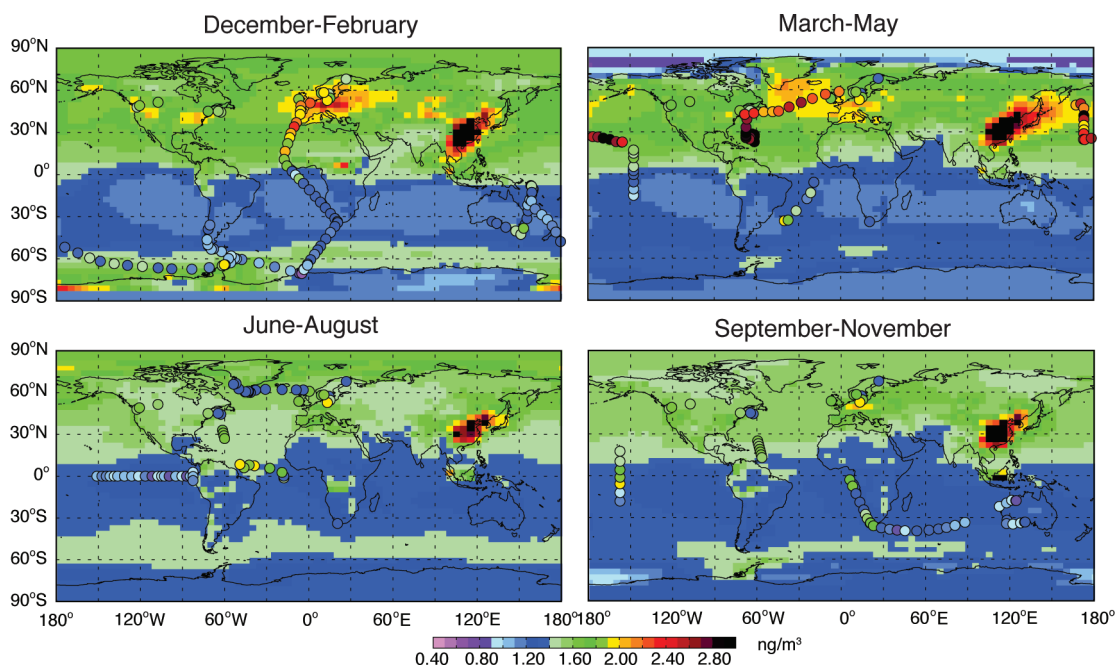


**FIGURE 4.** Mean Hg<sup>0</sup> concentrations in the atmospheric marine boundary layer (MBL) and terrestrial sites for different seasons. GEOS-Chem model values (background) are compared to cruise and land-based observations (circles) described in Kim and Fitzgerald (54), Soerensen et al. (50) and Selin et al. (5) and references therein.

$\text{m}^{-2}$ ), net primary productivity (NPP,  $\text{gC m}^{-2} \text{d}^{-1}$ ) and  $k_{\text{OX1}}$ ,  $k_{\text{RED1}}$ , and  $k_{\text{RED2}}$ . NPP values for this derivation were for the outer and shelf region of Chesapeake Bay characteristic of the measurement period (40). We further adjusted rate coefficients within observational confidence limits to be consistent with the ratio between photo-oxidation and photoreduction measured by Qureshi et al. (39), resulting in the following relationships implemented in our model:  $k_{\text{OX1}} = 6.6 \times 10^{-6} \times R$ ;  $k_{\text{RED1}} = 1.7 \times 10^{-6} \times R$ ;  $k_{\text{RED2}} = 4.5 \times 10^{-6} \times \text{NPP}$ . We also include a term for dark oxidation ( $k_{\text{OX2}} = 1.0 \times 10^{-7} \text{ s}^{-1}$ ) based on Lalonde et al. (21).

Spatial and seasonal variability in redox rates are modeled based on light attenuation in the surface mixed layer, the surface local shortwave radiation flux from GEOS-5, and global NPP distributions from MODIS satellite data (41). Light attenuation with depth is estimated from empirically determined effective light absorption coefficients for seawater, dissolved organic carbon (DOC) and pigments, and their respective concentrations (42) (SI Table S3). Pigment concentrations are derived from MODIS satellite data, while DOC is based on a global mean of  $1.5 \text{ mg L}^{-1}$  in the surface mixed layer, scaled by the distribution of global NPP to account for productivity related concentration differences (43).

**Sorption of  $\text{Hg}^{\text{II}}$  to Particles and Export Fluxes.** We model  $\text{Hg}^{\text{p}}$  removal from the surface ocean by linking  $\text{Hg}^{\text{II}}$  sorption to particulate matter and settling to organic carbon export fluxes (the ocean biological pump). The affinity of aqueous  $\text{Hg}^{\text{II}}$  for the solid phase is described using an empirically measured partition coefficient ( $K_{\text{D}}$ ,  $\text{L kg}^{-1}$ ):

$$K_{\text{D}} = \frac{C_{\text{s}}}{C_{\text{D}}} \quad (1)$$

Where  $C_{\text{s}}$  is the suspended particulate matter (SPM) concentration of  $\text{Hg}^{\text{II}}$  on a dry weight (mass/mass) basis ( $\text{pg kg}^{-1}$ ) and  $C_{\text{D}}$  is the filtered concentration (mass/volume) of  $\text{Hg}^{\text{II}}$  in seawater ( $\text{pg L}^{-1}$ ). The model re-equilibrates the  $\text{Hg}^{\text{II}}$  pool between the dissolved and solid phases at each time step, prior to calculating the reducible and nonreducible dissolved  $\text{Hg}^{\text{II}}$  pools.

We use a log  $K_{\text{D}}$  value based on NP and North Atlantic (NA) measurements ( $5.5 \pm 0.5$ ) (44, 45). Since no global data sets for SPM concentrations in ocean surface waters are available, we use integrated water column algal biomass derived from MODIS chlorophyll *a* data and statistical relationships from Uitz et al. (46) for subsurface algal productivity (see SI Section II). Settling fluxes of  $\text{Hg}^{\text{p}}$  are calculated using the parametrization described in Sunderland and Mason (24) for export of particulate organic carbon with depth and  $\text{Hg}^{\text{p}}$  to carbon (Hg:C) ratios. Spatially and temporally variable Hg:C ratios are calculated at each time step in the model (global mean of  $0.16 \text{ ng Hg per mg C}$ ) from the reservoir of  $\text{Hg}^{\text{p}}$  (derived from  $K_{\text{D}}$ ) and the standing stock of organic carbon in the surface ocean (SI Table S2).

## Results and Discussion

**Global Budget.** Figure 2 shows our global budget for Hg cycling in the surface ocean. Atmospheric deposition accounts for the largest fraction of Hg inputs to the surface ocean ( $18.5 \text{ Mmol y}^{-1}$ ). Entrainment of the mixed layer and Ekman pumping supply substantial amounts of  $\text{Hg}^{\text{II}}$  ( $10.0 \text{ Mmol y}^{-1}$ ),  $\text{Hg}^{\text{p}}$  ( $1.2 \text{ Mmol y}^{-1}$ ), and  $\text{Hg}^{\text{0}}$  ( $1.3 \text{ Mmol y}^{-1}$ ) from intermediate waters, accounting for 40% ( $12.5 \text{ Mmol y}^{-1}$ ) of the global total Hg inputs to the surface ocean. Inputs are balanced by  $\text{Hg}^{\text{0}}$  evasion ( $14.7 \text{ Mmol y}^{-1}$ ) and  $\text{Hg}^{\text{p}}$  removal ( $16.3 \text{ Mmol y}^{-1}$ ). Globally there is a net removal (sink) of  $3.8 \text{ Mmol Hg y}^{-1}$  to the subsurface ocean, mainly through particle-associated scavenging of  $\text{Hg}^{\text{p}}$ . Much of this  $\text{Hg}^{\text{p}}$  is remineralized in intermediate ocean waters.

Surface water  $\text{Hg}^{\text{0}}$  reflects the supply of reducible  $\text{Hg}^{\text{II}}$  complexes and the rates of photolytic and biotic redox reactions. Turnover of the dissolved  $\text{Hg}^{\text{II}}/\text{Hg}^{\text{0}}$  pools through photoreduction and photo-oxidation are rapid and dominate redox cycling except in environments where light is limited. Enhanced light penetration in oligotrophic areas with shallow mixed layers (e.g., seasonally in the Arctic, western Atlantic Ocean and western equatorial Pacific), means that photoreduction and photo-oxidation dominate dark redox processes where rate coefficients increase from a global mean  $10^{-5} \text{ s}^{-1}$  up to a maximum of  $10^{-4} \text{ s}^{-1}$  for reduction and  $10^{-3} \text{ s}^{-1}$  for oxidation. Biotic reduction is more important in highly productive regions (e.g., eastern Atlantic and eastern equatorial Pacific) where reaction rates increases from a global mean of  $10^{-7} \text{ s}^{-1}$  up to  $10^{-6} \text{ s}^{-1}$  and photo-oxidation and photoreduction decrease to  $10^{-6} \text{ s}^{-1}$  due to limited light penetration through the mixed layer.

Our modeled  $\text{Hg}^{\text{0}}$  evasion falls within 90% confidence limits of previous estimates that ranged between 9.7 and  $20.7 \text{ Mmol y}^{-1}$  (24) and is in the same range as the previous GEOS-Chem ocean model ( $14.1 \text{ Mmol y}^{-1}$ ). Figure 2 shows the subsurface ocean contributes a substantial fraction of the Hg present in the mixed layer. These results contrast those of Strode et al. (2) who predicted that atmospheric deposition accounted for almost all (89%) of the  $\text{Hg}^{\text{II}}$  inputs. Better resolved intermediate water Hg concentrations in our simulation account for this difference.

### Model Comparisons with Seawater Measurements.

Figure 3A and B shows a comparison of modeled total Hg and  $\text{Hg}^{\text{0}}$  in the global oceans with available surface ocean measurement data. Modeled seawater concentrations are highly variable ranging from  $<0.01 \text{ pM}$  to  $>0.5 \text{ pM}$  for  $\text{Hg}^{\text{0}}$  and  $<0.1 \text{ pM}$  to  $>2.5 \text{ pM}$  for total Hg depending on month and region. Seawater measurements of aqueous total Hg and  $\text{Hg}^{\text{0}}$  are extremely limited; thus data shown in Figure 3 span more than two decades compared to model results for 2008 (see also SI Figure S1–S2). Comparing model results from the Atlantic and Pacific Oceans with data from the decade preceding our simulation (1999–2008) reveals reasonable consistency with total Hg ( $r = 0.95$ ) and  $\text{Hg}^{\text{0}}$  ( $r = 0.54$ ). However, there is little agreement between 2008 model results and measurements for the prior decade (1988–1998) of total Hg ( $r = 0.24$ ) and  $\text{Hg}^{\text{0}}$  ( $r = -0.51$ ). Temporal trend data are insufficient to indicate whether these differences between observed (1988–1998) and modeled (2008) values are attributable to changes in environmental concentrations. The model does not capture elevated total Hg and  $\text{Hg}^{\text{0}}$  concentrations measured in some coastal and shelf regions such as the Hudson Bay region (Figure 3A and B). The predicted coastal/shelf Hg concentrations may be low because the model does not presently include Hg inputs from rivers, which other modeling studies suggest substantially increase near-shore concentrations (24, 47). Additional model sensitivity analyses are described in the SI.

### High Concentrations in the North Atlantic (NA) Ocean.

Figure 3A and B show high concentrations of total Hg and  $\text{Hg}^{\text{0}}$  in the NA. In addition to atmospheric deposition (Figure 3C), the NA receives large Hg contributions from subsurface waters through Ekman pumping and entrainment of intermediate waters (Figure 3D). Subsurface Hg entrainment is enhanced in the NA compared to other regions because wind-driven winter mixing increases the mixed layer depth from  $<50 \text{ m}$  in the summer to over  $600 \text{ m}$  and intermediate waters are relatively enriched in Hg compared to other oceans (Figure 1). Sunderland and Mason (24) suggested that high relative Hg concentrations in NA subsurface waters (12) results from earlier peaks in anthropogenic emissions concentrated on the east coast of North America and Europe. Their results also showed a lag time of several decades in the NA before historical inputs are fully reflected by seawater

concentrations. Peaks in anthropogenic Hg emissions in the 1960–70s are evident in both sediment cores from eastern North America and historical inventories (e.g., refs 48, 49).

Net Hg<sup>0</sup> evasion (Figure 3F) reflects the speed of air–sea exchange and Hg<sup>0</sup> supersaturation relative to the atmosphere. Combined Hg inputs and losses from the mixed layer (Figure 3C–3F) determine reducible Hg<sup>II</sup> supply and Hg<sup>0</sup> concentrations. Although globally the ocean is a net Hg sink, much of the NA is a net source to the atmosphere (Figure 3F). In addition to large inputs from intermediate water entrainment, Ekman pumping and the speed of air–sea exchange are enhanced by high winds during winter months in the NA when losses from Hg<sup>p</sup> settling are low (Figure 3E). Thus, much of the evaded Hg<sup>0</sup> likely originates from legacy Hg that has accumulated in subsurface waters.

**Global Distribution of Hg<sup>0</sup> Evasion.** Figure 2F shows the global distribution of modeled net annual Hg<sup>0</sup> evasion. The current simulation with atmospheric Hg<sup>0</sup> oxidation by Br atoms rather than OH/O<sub>3</sub> (25) shifts Hg<sup>II</sup> deposition from the subtropics to high latitudes (Figure 3C). This shift results in higher evasion rates in the Southern Ocean, NA and NP relative to the previous simulation (2). Substantial Hg inputs to the mixed layer through entrainment and Ekman pumping are apparent in equatorial upwelling regions (Figure 3D), although these inputs are partially offset through losses by Hg<sup>p</sup> settling (Figure 3E). Net losses through entrainment/detrainment and Ekman pumping (Figure 3D) occur in some areas of the South Pacific and Southern Ocean where subsurface Hg concentrations are lowest globally (Figure 1). Nutrient-like depletion of inorganic Hg concentrations occurs in highly productive regions of equatorial Atlantic (Figure 3E), which explains the low concentrations observed in this region (Figure 3A and B), and resulting low evasion rates.

**Seasonal Variability in MBL Concentrations.** Figure 4 shows simulated and observed Hg<sup>0</sup> concentrations in the atmospheric MBL for different seasons. Model results show the impacts of high NA ocean emissions (0.6 nmol m<sup>-2</sup> d<sup>-1</sup>) as peak MBL concentrations in the winter and early spring. In contrast, net Hg<sup>0</sup> deposition occurs during summer months (SI Figure S4). This pattern matches seasonal trends in monthly cruise measurements of MBL TGM concentrations ( $r = 0.82$ ), as described by Soerensen et al. (50), that peak in the late winter and are lowest in the summer (Figure 5A).

Winter and early spring NA Hg<sup>0</sup> evasion rates are particularly high because of elevated Hg<sup>II</sup> entrainment into the mixed layer, enhanced Ekman pumping, and high winds increase air–sea exchange rates (SI Figure S4). Conversely, in the summer and early fall mixed layer depth decreases (detrainment) and the reservoirs of Hg<sup>0</sup> and reducible Hg<sup>II</sup> are more limited, lowering seawater Hg<sup>0</sup> saturation values relative to the atmosphere (SI Figure S4). In addition, enhanced productivity during summer months increases scavenging of Hg<sup>p</sup> and can lower evasion by depleting the reducible Hg<sup>II</sup> pool. Pronounced seasonality in NA oceanic evasion does not compromise the model's ability to capture trends at inland measurement sites (Figure 4), as discussed in Holmes et al. (25).

Enhanced modeled Pacific Ocean MBL concentrations are found primarily during the spring months, which also agrees with cruise measurements. However, oceanic emissions do not explain all elevated NP MBL observations (Figure 4). Seasonal differences in modeled NP Hg<sup>0</sup> evasion are not as pronounced due to lower subsurface Hg concentrations and less pronounced vertical mixing. For example, during winter months vertical mixing with intermediate waters accounts for 75% of Hg inputs to the NA surface waters compared to 30% for the NP. Elevated western NP MBL observations are therefore likely dominated by outflow from anthropogenic emissions in East Asia (51).

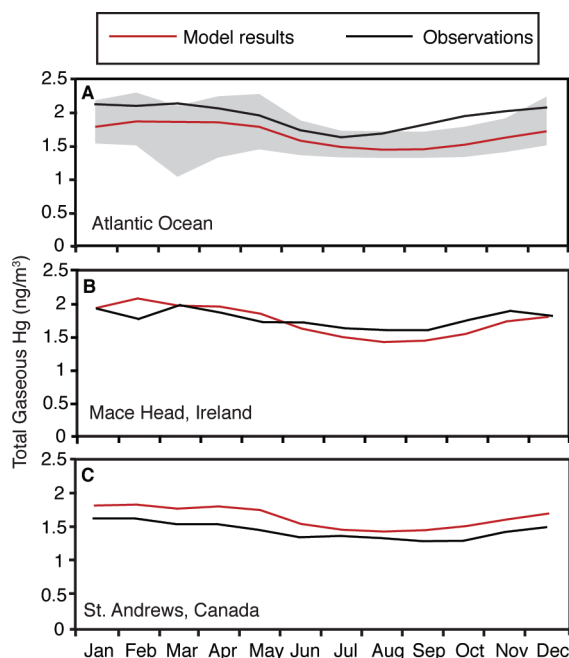


**FIGURE 5.** Seasonal variation of total gaseous Hg (TGM) in the marine boundary layer (MBL). Panel (A) shows the Atlantic Ocean (60:0W, 15:65N) and mean of all cruise measurements in the Atlantic. Gray areas indicate monthly maximum and minimum values. Panels (B) and (C) show values at the coastal sites Mace Head, Ireland and St. Andrews, Canada. Data sources are described in Soerensen et al. (50) and Selin et al. (5) and references therein.

Figure 5 compares the phase and amplitude of the seasonal cycle in MBL TGM concentrations with Atlantic Ocean measurements and selected coastal monitoring stations. The improved ocean model reproduces the seasonal cycle seen at most coastal monitoring sites (Birkenes, Pallas, Reiffel Island, Mace Head and St. Andrews) (e.g., Figure 5B and C). Both modeled and measured winter and spring MBL concentrations at marine stations shown in Figure 5 are higher than those seen at rural sites on the adjacent continents (25).

Results from our improved surface ocean model reinforce the importance of air–sea exchange processes as a control on MBL TGM concentrations. Oceanic emissions account for greater than 40% of MBL Hg levels in virtually all marine regions (SI Figure S5). Although the new model better captures seasonality and enhanced Northern Hemisphere MBL TGM concentrations relative to previous work (2), concentrations remain lower than some cruise measurements in the Atlantic Ocean (Figure 5A). Additional increases in evasion are not supported by model observational constraints based on terrestrial monitoring stations shown in Figure 4. We hypothesize that temporal changes in direct anthropogenic emissions and subsurface ocean concentrations has resulted in dynamic oceanic emissions and may help to explain observed MBL concentrations over the past two decades.

### Acknowledgments

We acknowledge financial support for this work from the Electric Power Research Institute (EPRI), NERI-University of Aarhus, the Oticon Foundation, and the Hakun Lund foundation. R.P.M. acknowledges support from NSF Chemical Oceanography (OCE-728750). A.L.S. thanks Ole John Nielsen for mediating contact with SEAS, Harvard University.

### Supporting Information Available

Additional information including Figures S1–S5 and Tables S1–S4. This material is available free of charge via the Internet at <http://pubs.acs.org>.

## Literature Cited

- (1) Selin, N.; Jacob, D.; Yantosca, R.; Strode, S.; Jaegle, L.; Sunderland, E. Global 3-D land-ocean-atmosphere model for mercury: Present-day versus preindustrial cycles and anthropogenic enrichment factors for deposition. *Global Biogeochem. Cycles* **2008**, *22*, GB2011.
- (2) Strode, S.; Jaegle, L.; Selin, N.; Jacob, D.; Park, R.; Yantosca, R.; Mason, R.; Slemr, F. Air-sea exchange in the global mercury cycle. *Global Biogeochem. Cycles* **2007**, *21*, GB1017.
- (3) Sunderland, E. M. Mercury exposure from domestic and imported estuarine and marine fish in the U.S. seafood market. *Environ. Health Perspect.* **2007**, *115* (2), 235–242.
- (4) Dastoor, A.; Larocque, Y. Global circulation of atmospheric mercury: a modelling study. *Atmos. Environ.* **2004**, *38*, 147–161.
- (5) Selin, N. E.; Jacob, D. J.; Park, R. J.; Yantosca, R. M.; Strode, S.; Jaegle, L.; Jaffe, D. Chemical cycling and deposition of atmospheric mercury: Global constraints from observations. *J. Geophys. Res., [Atmos.]* **2007**, *112*, D02308.
- (6) Seigneur, C.; Jayaraghavan, K.; Lohman, K.; Karamchandani, P.; Scott, C. Global source attribution for mercury deposition in the United States. *Environ. Sci. Technol.* **2004**, *38*, 555–569.
- (7) Temme, C.; Slemr, F.; Ebinghaus, R.; Einax, J. Distribution of mercury over the Atlantic Ocean in 1996 and 1999–2001. *Atmos. Environ.* **2003**, *37*, 1889–1897.
- (8) Slemr, F.; Brunke, E.-G.; Ebinghaus, R.; Temme, C.; Munthe, J.; Wangberg, I.; Schroeder, W.; Steffen, A.; Bernd, T. Worldwide trend of atmospheric mercury since 1977. *Geophys. Res. Lett.* **2003**, *30* (10), 1516.
- (9) Laurier, F.; Mason, R.; Whalin, L.; Kato, S. Reactive gaseous mercury formation in the North Pacific Ocean's marine boundary layer: a potential role of halogen chemistry. *J. Geophys. Res.* **2003**, *108* (D17), 4529.
- (10) Sunderland, E. M.; Krabbenhoft, D. P.; Moreau, J. W.; Strode, S. A.; Landing, W. M. Mercury sources, distribution, and bioavailability in the North Pacific Ocean: Insights from data and models. *Global Biogeochem. Cycles* **2009**, *23*, Art. No. GB2010.
- (11) Gill, G.; Fitzgerald, W. F. Vertical mercury distributions in the oceans. *Geochim. Cosmochim. Acta* **1988**, *52*, 1719–1728.
- (12) Laurier, F.; Mason, R.; Gill, G.; Whalin, L. Mercury distribution in the North Pacific Ocean—20 years of observations. *Mar. Chem.* **2004**, *90* (1–4), 3–19.
- (13) Andersson, M. E.; Sommar, J.; Gardfeldt, K.; Lindqvist, O. Enhanced concentrations of dissolved gaseous mercury in the surface waters of the Arctic Ocean. *Mar. Chem.* **2008**, *110* (3–4), 190–194.
- (14) Mason, R.; Lawson, N.; Sheu, G.-R. Mercury in the Atlantic Ocean: factors controlling air-sea exchange of mercury and its distribution in upper waters. *Deep-Sea Res. II* **2001**, *48*, 2829–2853.
- (15) Mason, R.; Rolfhus, K.; Fitzgerald, W. Methylated and elemental mercury cycling in surface and deep-ocean waters of the North Atlantic. *Water, Air, Soil Pollut.* **1995**, *80* (1–4), 665–677.
- (16) Rolfhus, K. R.; Fitzgerald, W. F. Mechanisms and temporal variability of dissolved gaseous mercury production in coastal seawater. *Mar. Chem.* **2004**, *90* (1–4), 125–136.
- (17) Whalin, L.; Kim, E.; Mason, R. Factors influencing the oxidation, reduction, methylation and demethylation of mercury species in coastal waters. *Mar. Chem.* **2007**, *107*, 278–294.
- (18) Amyot, M.; Gill, G. A.; Morel, F. M. M. Production and loss of dissolved gaseous mercury in coastal seawater. *Environ. Sci. Technol.* **1997**, *31* (12), 3606–3611.
- (19) Amyot, M.; Lean, D. R. S.; Poissant, L.; Doyon, M.-R. Distribution and transformation of elemental mercury in the St. Lawrence River and Lake Ontario. *Can. J. Fish. Aquat. Sci.* **2000**, *57* (Suppl. 1), 155–163.
- (20) Gardfeldt, K.; Feng, X. B.; Sommar, J.; Lindqvist, O. In *Total Gaseous Mercury Exchange between Air and Water at River and Sea Surfaces in Swedish Coastal Regions*; Pergamon-Elsevier Science Ltd New York, 2001; pp 3027–3038.
- (21) Lalonde, J.; Amyot, M.; Kraepiel, A.; Morel, F. Photooxidation of Hg(0) in artificial and natural waters. *Environ. Sci. Technol.* **2001**, *35*, 1367–1372.
- (22) Lalonde, J. D.; Amyot, M.; Orvoine, J.; Morel, F. M. M.; Auclair, J. C.; Ariya, P. A. Photoinduced oxidation of Hg-0 (aq) in the waters from the St. Lawrence estuary. *Environ. Sci. Technol.* **2004**, *38* (2), 508–514.
- (23) Zafriou, O. C.; True, M. B.; Hayon, E., Consequences of OH radical reaction in sea water: Formation and decay of Br<sup>2-</sup> ion radical. In *Photochemistry of Environmental Aquatic Systems*; Zika, R. G., Cooper, W. J., Eds.; American Chemical Society: Washington, DC, 1987; pp 89–105.
- (24) Sunderland, E. M.; Mason, R. Human impacts on open ocean mercury concentrations. *Global Biogeochem. Cycles* **2007**, *21*, GB4022.
- (25) Holmes, C. D.; Jacob, D. J.; Corbitt, E. S.; Mao, J.; Yang, X.; Talbot, R.; Slemr, F. Global atmospheric model for mercury including oxidation by bromine atoms. *Atmos. Chem. Phys. Discuss.* **2010**, *10*, 19845–19900.
- (26) Montegut, C. D.; Madec, G.; Fischer, A. S.; Lazar, A.; Iudicone, D. Mixed layer depth over the global ocean: An examination of profile data and a profile-based climatology. *J. Geophys. Res., [Oceans]* **2004**, *109* (C12), 20.
- (27) Pacyna, E.; Pacyna, J.; Steenhuisen, F.; Wilson, S. Global anthropogenic mercury emission inventory for 2000. *Atmos. Environ.* **2006**, *40*, 4048–4063.
- (28) Streets, D. G.; Zhang, Q. Projections of global mercury emissions in 2050. *Environ. Sci. Technol.* **2009**, *43* (8), 2983–2988.
- (29) Pirrone, N.; Cinnirella, S.; Feng, X.; Finkelman, R.; Friedli, H. R.; Leaner, J.; Mason, R. P.; Mukherjee, A. B.; Stracher, G.; Streets, D. G.; Telmer, K. Global mercury emissions to the atmosphere from anthropogenic and natural sources. *Atmos. Chem. Phys. Discuss.* **2010**, *10*, 4719–4752.
- (30) Nightingale, P.; Malin, G.; Law, C.; AJ, W.; Liss, P.; Liddicoat, M.; Boutin, J.; Upstill-Goddard, R. In situ evaluation of air-sea gas exchange parameterizations using novel conservative and volatile tracers. *Global Biogeochem. Cycles* **2000**, *14* (1), 373–387.
- (31) Andersson, M. E.; Gardfeldt, K.; Wangberg, I.; Stromberg, D. Determination of Henry's law constant for elemental mercury. *Chemosphere* **2008**, *73* (4), 587–592.
- (32) Poissant, L.; Amyot, M.; Pilote, M.; Lean, D. Mercury water-air exchange over the upper St. Lawrence River and Lake Ontario. *Environ. Sci. Technol.* **2000**, *2000* (34), 3069–3078.
- (33) Wilke, C. R.; Chang, P. Correlation of diffusion coefficients in dilute solutions. *AIChE J.* **1955**, *1* (2), 264–270.
- (34) Kirk, J. L.; St. Louis, V.; Hintelmann, H.; Lehnher, I.; Else, B.; Poissant, L. Methylated mercury species in marine waters of the Canadian High and Sub Arctic. *Environ. Sci. Technol.* **2008**, *42* (22), 8367–8373.
- (35) O'Driscoll, N.; Siciliano, S.; Lean, D.; Amyot, M. Gross photoreduction kinetics of mercury in temperate freshwater lakes and rivers: Application to a general model of DGM dynamics. *Environ. Sci. Technol.* **2006**, *40*, 837–843.
- (36) Stumm, W.; Morgan, J. J., *Aquatic Chemistry: Chemical Equilibria and Rates in Natural Waters*, 3rd ed.; John Wiley & Sons, Inc.: New York, NY, 1996; p 1022.
- (37) Mason, R. P.; Morel, F. M. M.; Hemond, H. F. The role of microorganisms in elemental mercury formation in natural waters. *Water, Air, Soil Pollut.* **1995**, *80*, 775–787.
- (38) Poulain, A. J.; Ni Chadhain, S. M.; Ariya, P. A.; Amyot, M.; Garcia, E.; Campbell, P. G. C.; Zylstra, G. J.; Barkay, T. Potential for mercury reduction by microbes in the high arctic. *Appl. Environ. Microbiol.* **2007**, *73* (7), 2230–2238.
- (39) Qureshi, A.; O'Driscoll, N. J.; MacLeod, M.; Neuhold, Y. M.; Hungerbuhler, K. Photoreactions of mercury in surface ocean water: gross reaction kinetics and possible pathways. *Environ. Sci. Technol.* **2010**, *44* (2), 644–649.
- (40) Cerco, C. Phytoplankton kinetics in the Chesapeake Bay Eutrophication Model. *Water Qual. Ecosyst. Model.* **2000**, *1*, 5–49.
- (41) Behrenfeld, M. J.; Falkowski, P. G. Photosynthetic rates derived from satellite-based chlorophyll concentration. *Limnol. Oceanogr.* **1997**, *42* (1), 1–20.
- (42) Wozniak, B.; Dera, J., *Light Absorption in Sea Water*; Springer: New York, NY, 2007; p 456.
- (43) Chester, R., *Marine Geochemistry*, 2nd Ed.; Blackwell Science Ltd.: Berlin, Germany, 2003; p 506.
- (44) Mason, R. P.; Fitzgerald, W. The distribution and cycling of mercury in the equatorial Pacific Ocean. *Deep-Sea Res., Part 1* **1993**, *40* (9), 1897–1924.
- (45) Mason, R.; Rolfhus, K.; Fitzgerald, W. Mercury in the North Atlantic. *Mar. Chem.* **1998**, *61*, 37–53.
- (46) Uitz, J.; Claustre, H.; Morel, A.; Hooker, S. B. Vertical distribution of phytoplankton communities in open ocean: An assessment based on surface chlorophyll. *J. Geophys. Res., [Oceans]* **2006**, *111* (C8), 23.
- (47) Sunderland, E. M.; Dalziel, J.; Heyes, A.; Branfireun, B. A.; Krabbenhoft, D. P.; Gobas, F. Response of a macrotidal estuary to changes in anthropogenic mercury loading between 1850 and 2000. *Environ. Sci. Technol.* **2010**, *44* (5), 1698–1704.

- (48) Sunderland, E. M.; Cohen, M.; Selin, N.; Chmura, G. Reconciling models and measurements to assess trends in atmospheric mercury deposition. *Environ. Pollut.* **2008**, *156*, 526–535.
- (49) Sunderland, E. M.; Chmura, G. L. An inventory of historical mercury pollution in Maritime Canada: Implications for present and future contamination. *Sci. Total Environ.* **2000**, *256* (1), 39–57.
- (50) Soerensen, A. L.; Skov, H.; Jacob, D. J.; Soerensen, B. T.; Johnson, M. S., Global concentrations of gaseous elemental mercury and reactive gaseous mercury in the marine boundary layer. *Environ. Sci. Technol.* **2010**, *44*, 7425–7430.
- (51) Strode, S.; Jaegle, L.; Jaffe, D.; Swartzendruber, P.; Seline, N.; Holmes, C.; Yantosca, R., Trans-Pacific transport of mercury. *J. Geophys. Res., [Atmos.]* **2008**, *113*, D15305, DOI: 10.1029/2007JD009428.
- (52) Mason, R.; Sullivan, K. A. The distribution and speciation of mercury in the South and equatorial Atlantic. *Deep-Sea Res., Part II* **1999**, *46*, 937–956.
- (53) Lamborg, C. H.; Hammerschmidt, C. R.; Saito, M.; Goepfert, T.; Lam, P. J., Mercury methylation in the gyre and Benguela upwelling regions of the tropical South Atlantic Ocean. In *9th International Conference on Mercury as a Global Pollutant*; Guiyang, China, June 7–12, 2009.
- (54) Kim, J.; Fitzgerald, W. Sea-Air partitioning of mercury in the equatorial Pacific Ocean. *Science* **1986**, *231* (4742), 1131–1133.

ES102032G

## SUPPORTING INFORMATION

# An Improved Global Model for Air-Sea Exchange of Mercury: High Concentrations Over the North Atlantic

*Anne L. Soerensen<sup>\*†‡</sup>, Elsie M. Sunderland<sup>‡</sup>, Christopher D. Holmes<sup>‡</sup>, Daniel J. Jacob<sup>‡</sup>, Robert Yantosca<sup>‡</sup>, Henrik Skov<sup>†</sup>, Jesper H. Christensen<sup>†</sup>, Sarah A. Strode<sup>§</sup>, and Robert P. Mason<sup>||</sup>*

<sup>†</sup>National Environmental Research Institute, Aarhus University, Frederiksborgvej 399, DK-4000 Roskilde, Denmark

<sup>‡</sup>Harvard University, School of Engineering and Applied Sciences and Department of Earth and Planetary Sciences, Cambridge MA, 02138, USA

<sup>§</sup>Department of Atmospheric Sciences, University of Washington, Seattle, WA, 98195 USA

<sup>||</sup>University of Connecticut, Department of Marine Sciences, 1080 Shennecossett Road, Groton, CT, 0634, USA

<b>Contents</b>		<b>Page(s)</b>
Section I	Model Sensitivity Analyses	2
Section II	Supplemental Results	3-6
Section III	Model Updates and Formulation	6-11
Section IV	References Cited	12-14
Figure S1	Comparison of monthly modeled and observed seawater total inorganic Hg	3
Figure S2	Comparison of modeled and observed seawater Hg <sup>0</sup>	3
Figure S3	Modeled seasonal surface water Hg <sup>0</sup> saturation values for 2008	4
Figure S4	Seasonal variability in modeled oceanic evasion for 2008	5
Figure S5	Modeled contribution of oceanic Hg <sup>0</sup> emissions to marine boundary Hg <sup>0</sup> concentrations	6
Table S1	Model differential equations	7
Table S2	Particle associated mercury reservoirs and fluxes	7
Table S3	Redox reactions	10
Table S4	Gas-exchange parameterization	11

## Section I: Model Sensitivity Analyses

We performed a variety of sensitivity analysis to help prioritize future experimental data needs. The reducible  $\text{Hg}^{\text{II}}$  pool is rarely measured in studies collecting data on gross reaction kinetics (1) and should be a priority for future research because  $\text{Hg}^0$  evasion increases/decreases proportionally to this pool in our simulation. Other studies have suggested that the diffusivity of  $\text{Hg}^0$  in seawater (2) is overestimated by standard calculation methods like Wilke-Chang (3), which could lead to low retention of  $\text{Hg}^0$  in the surface waters. However, implementing the experimentally based diffusivity term for  $\text{Hg}^0$  proposed by Kuss et al. (4) in our model simulation only increases aqueous  $\text{Hg}^0$  concentrations by 5% and results in a decrease in global net evasion of 14%.

We analyzed the sensitivity of modeling results to several gas transfer models. Using the gas transfer scheme developed by Liss and Merlivat (5), generally accepted as a low-end estimate, results in a 30% reduction in modeled global evasion compared to our standard simulation based on Nightingale et al. (6) but does not substantially change aqueous  $\text{Hg}^0$  concentrations. Several ecosystem-scale studies have shown  $\text{Hg}^0$  evasion flux estimates typically also vary by approximately 30%, depending on the choice of gas transfer model (7-9). Our results suggest that the Nightingale parameterization (6) that uses a quadratic relationship between evasion and wind speed is most appropriate because the linear dependence of evasion on wind speed in the Liss and Merlivat model (5) diminishes the modeled seasonal cycle of MBL Hg concentrations that is observed in the Northern Hemisphere (10).

## Section II: Supplemental Results

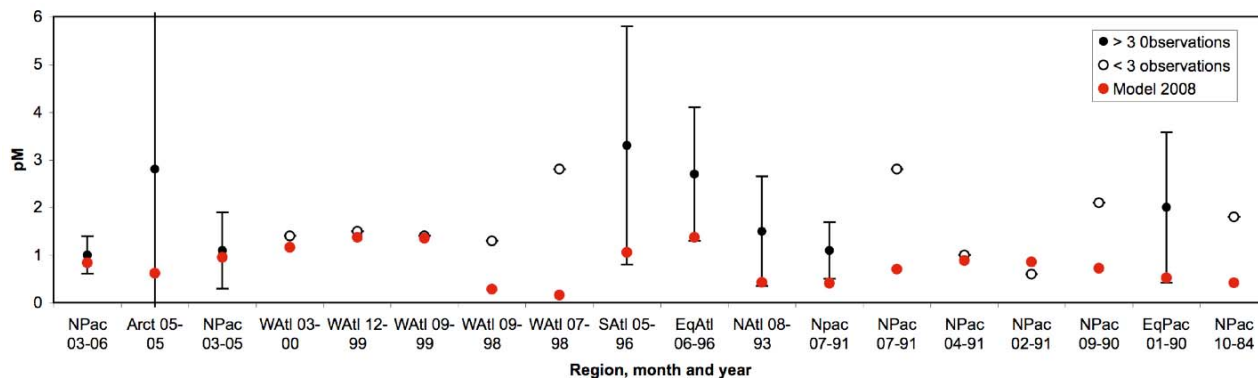


**Figure S1.** Comparison of monthly modeled (2008) and observed (various years) total inorganic Hg concentrations. Data sources are as follows: Pacific (11-16); Atlantic Ocean (16-19); Arctic Ocean (20).

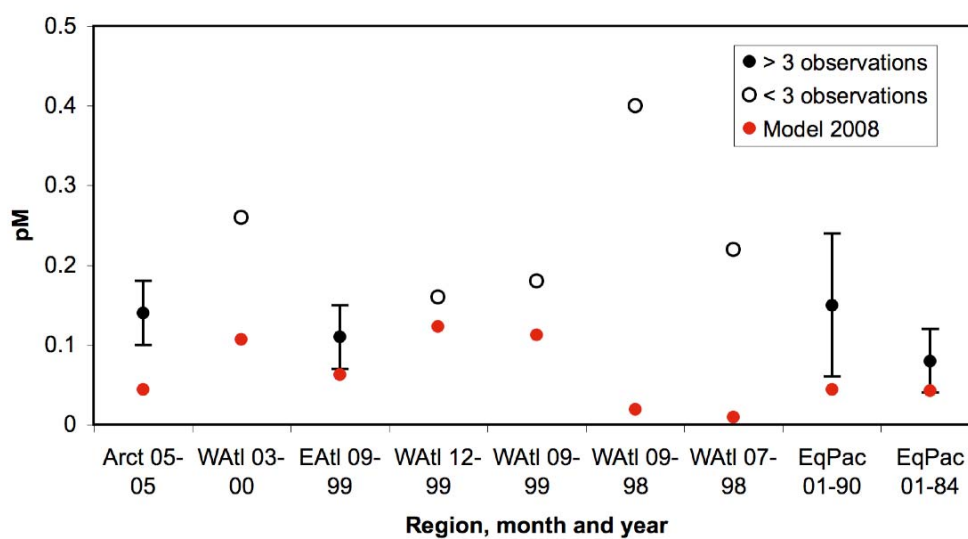


**Figure S2.** Comparison of monthly modeled (2008) and observed (various years) seawater  $Hg^0$  concentrations. Pacific Ocean: (13, 14, 21, 22); Atlantic Ocean (17, 23); Arctic Ocean: (20).

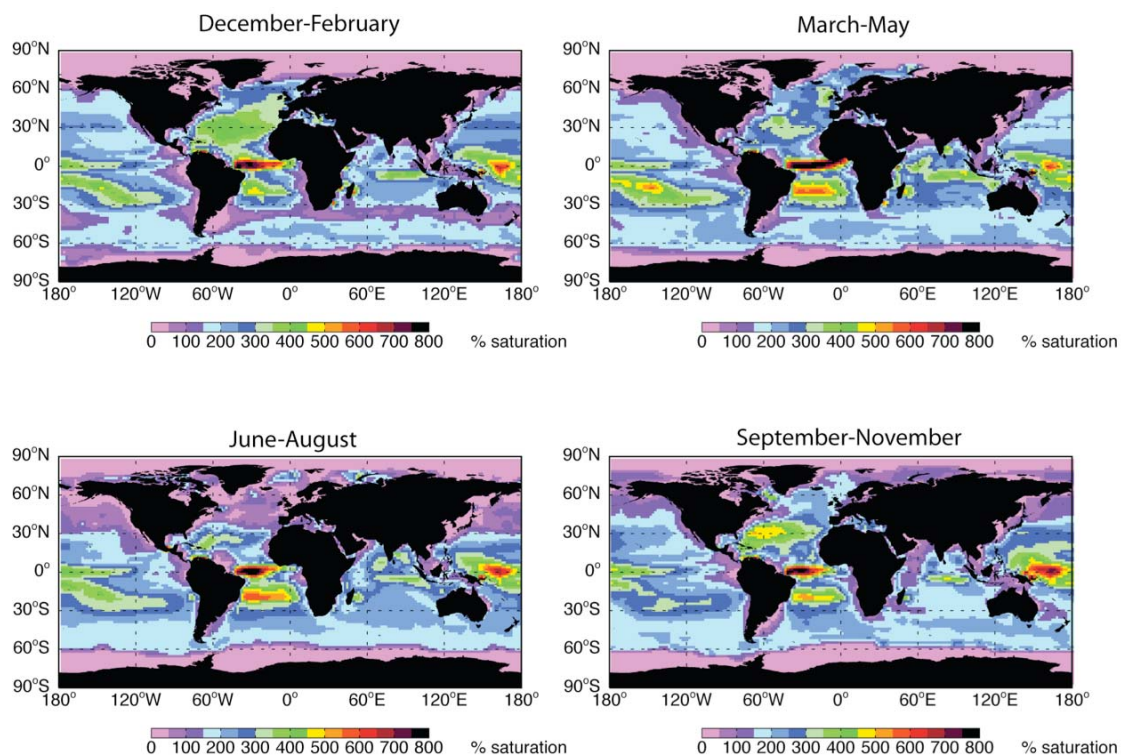


**Figure S3.** Modeled seasonal surface water  $\text{Hg}^0$  saturation values for 2008. The degree of saturation indicates the direction of the flux across the air-sea interface. Less than 100% indicates net deposition and greater than 100% indicates net evasion of  $\text{Hg}^0$ .

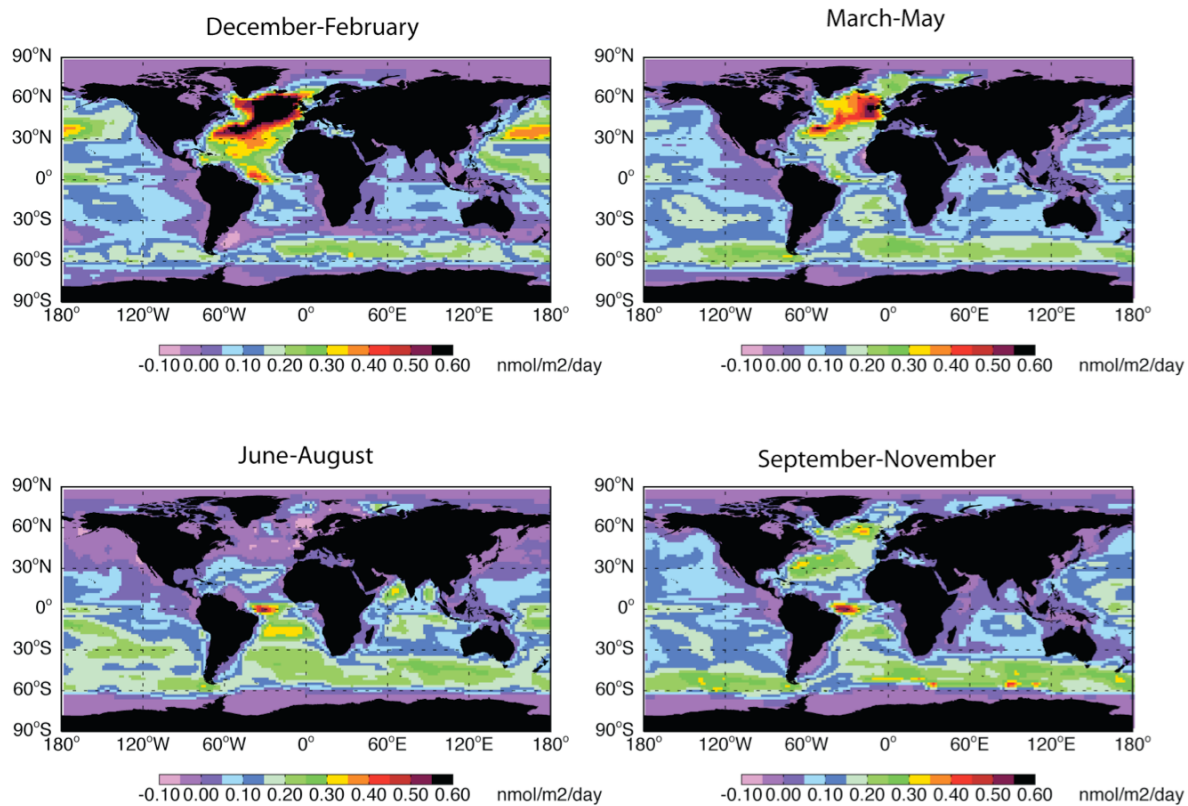


**Figure S4.** Seasonal variability in modeled oceanic  $Hg^0$  evasion for 2008.

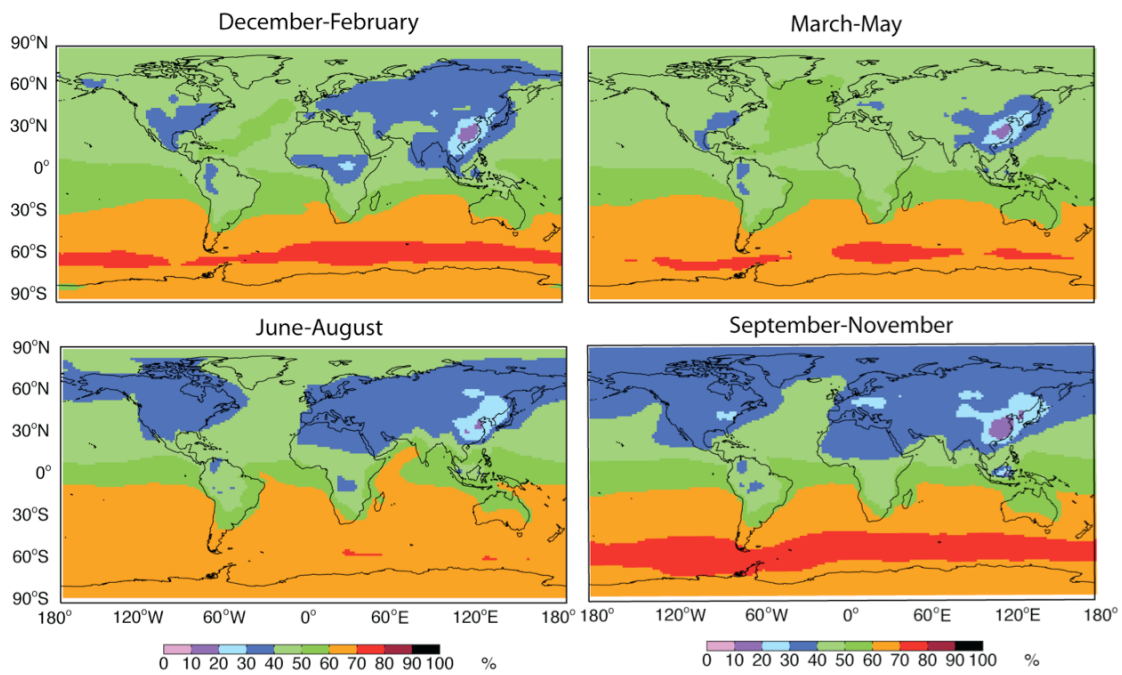


**Figure S5.** Modeled contribution of oceanic  $\text{Hg}^0$  evasion to marine boundary  $\text{Hg}^0$  concentrations.

### Section III: Model Updates and Formulation

**Table S1.** Model differential equations

Change in Hg <sup>0</sup> mass over time ( <i>dt</i> )	$\frac{dM_{Hg^0}}{dt} = M_{Ek}^{Hg^0} \pm M_{ent}^{Hg^0} \pm M_{ev} - k_{ox}M_{Hg^0} + k_r\phi_F\alpha_rM_{Hg^{II}}$	
Change in Hg <sup>II</sup> mass over time ( <i>dt</i> )	$\frac{dM_{Hg^{II}}}{dt} = M_a + M_{up}^{Hg^{II}} \pm M_{ent}^{Hg^{II}} - M_p + k_{ox}M_{Hg^0} - k_r\phi_F\alpha_rM_{Hg^{II}}$	
$M_a$ (kg)	Deposition of Hg to the ocean surface	
$M_{ent}$ (kg)	Mass of mercury species introduced or removed due to deep convection or shoaling of the mixed-layer	
$M_{Ek}$ (kg)	Wind-driven mass transfer of mercury species due to Ekman pumping	
$M_{ev}$ (kg)	Mass of Hg <sup>0</sup> evaded from the ocean to the atmosphere	
$M_p$ (kg)	Flux of Hg <sup>II</sup> lost from mixed layer with sinking particles	
$M_{Hg(0)}$ (kg)	Reservoir of Hg <sup>0</sup> in the surface mixed layer	
$M_{Hg(II)}$ (kg)	Reservoir of Hg <sup>II</sup> in the surface mixed layer	
$k_{ox}$ (s <sup>-1</sup> )	Hg <sup>0</sup> oxidation rate	$k_{ox1} + k_{ox2}$
$k_r$ (s <sup>-1</sup> )	Reduction rate of reducible pool of Hg <sup>II</sup>	$k_{red1} + k_{red2}$
$\phi_F$ (unitless)	Hg <sup>II</sup> fraction in the dissolved phase	$1/(1 + K_D SPM)$
$\alpha_r$ (unitless)	Reducible fraction of the filtered Hg <sup>II</sup> pool	0.40 (19, 24, 25)

**Table S2.** Particle associated mercury reservoirs and fluxes.

$M_{Hg^p}$ (kg)	Hg <sup>II</sup> mass in the particulate phase	$(1 - \phi_F)M_{Hg^{II}}$
$K_D$ (L kg <sup>-1</sup> )	Seawater partition coefficient for Hg <sup>II</sup>	$3.16 \times 10^5$ (14, 19)
$C_{SPM}$ (kg L <sup>-1</sup> )	Concentration of suspended particles	$10^3(C_{OC} \cdot M_{wet} \cdot A_w)/z_{MLD}$
$z_{MLD}$ (m)	Mixed layer depth	WOCE data assimilation (26)
$A_w$ (m <sup>2</sup> )	Water surface area	
$C_{OC}$ (mg m <sup>-2</sup> )	Standing stock of organic carbon in mixed layer	$C_{T-Chl} \cdot C_C : C_{Chl_a}$
$C_{T-Chl}$ (mg m <sup>-2</sup> )	Integrated water column pigment content	See text for derivation
$r_{C:Chla}$ (unitless)	Carbon to chlorophyll a ratio	80:1 (27)
$M_{wet}$ (unitless)	Conversion for wet weights of planktonic biomass	10 mg wet weight: mg carbon
$J_{orgC}$ (mg C m <sup>-2</sup> d <sup>-1</sup> )	Organic carbon flux out of the mixed layer	$0.1NPP^{1.77}z_{MLD}^n$
$NPP$ (mg C m <sup>-2</sup> d <sup>-1</sup> )	Net primary productivity	2003 MODIS satellite data (28)
$n$ (unitless)	Exponent describing relationship between declines in organic carbon flux due to mineralization in the water column with depth	-0.74 (29)
$r_{Hg:C}$ (unitless)	Hg <sup>P</sup> to organic carbon ratio in the mixed layer	$M_{Hg(P)}/(10^6 C_{OC} \cdot A_w)$
$M_p$ (kg)	Mass of Hg <sup>P</sup> lost from the mixed layer due to particle sinking	$J_{orgC} \cdot r_{Hg:C} \cdot A_w(dt)$

## **Method used for estimating suspended particulate matter concentrations**

No global data sets on SPM concentrations in the ocean mixed layer are available. We therefore estimate SPM concentrations in the surface mixed layer based on the standing biomass in the water column derived from MODIS satellite chlorophyll a ( $C_{Chla}$ ,  $\text{mg m}^{-3}$ ) concentrations (<http://oceancolor.gsfc.nasa.gov/ftp.html>) for the year 2003. We calculate the water column integrated pigment content within the euphotic layer ( $C_{T-Chl}$ ,  $\text{mg m}^{-2}$ ) based on the statistical fits for subsurface algal productivity in the ocean developed by Morel and Berthon (30) and updated by Uitz et al. (31).

These equations are as follows:

### 1. STRATIFIED WATERS

For stratified waters in low and mid latitude stations, where  $C_{Chla} \leq 1.0 \text{ mg m}^{-3}$

$$(1) \quad C_{T-Chl} = 36.1 C_{Chla}^{0.357}$$

For stratified waters in low and mid latitude stations, where  $C_{Chla} \geq 1.0 \text{ mg m}^{-3}$

$$(2) \quad C_{T-Chl} = 37.7 C_{Chla}^{0.615}$$

### 2. WELL-MIXED WATERS

For well-mixed waters at high latitudes:

$$(3) \quad C_{T-Chl} = 42.1 C_{Chla}^{0.538}$$

Waters are defined as well-mixed if  $z_{eu}/z_{MLD} < 1$   
Conversely, if  $z_{eu}/z_{MLD} > 1$  then the waters are considered stratified.

Where,

$z_{eu}$  is the euphotic depth and is defined as the depth where the PAR irradiance is 1% of its value at the surface.

$z_{MLD}$  (m) is the mixed layer depth derived from de Boyer Montegut et al. (26) from the National Oceanographic Data Center (NODE), World Ocean Circulation Experiment (WOCE) database, and the ARGO program (available: <http://www.locean-ipsl.upmc.fr/~cdblod/mlld.html>)

$C_{T-Chl}$  and  $z_{eu}$  are calculated iteratively in the model to determine whether waters are stratified or well mixed and the appropriate equations for  $C_{T-Chl}$ .

$z_{eu}$  is derived as a function of  $C_{T-Chl}$  by Morel and Maritorena (32):

$$(4) \quad z_{eu} = 912 C_{T-Chl}^{-0.839} \text{ when } 10 \text{ m} < z_{eu} < 102 \text{ m and } C_{T-Chl} > 13.65 \text{ mg m}^{-2}$$

$$(5) \quad z_{eu} = 426.3 C_{T-Chl}^{-0.547} \text{ when } 102 \text{ m} < z_{eu} < 180 \text{ m and } C_{T-Chl} < 13.65 \text{ mg m}^{-2}$$

We calculate the standing stock of organic carbon ( $C_{OC}$ ,  $\text{mg m}^{-2}$ ) from the integrated water column pigment content ( $C_{T-Chl}$ ,  $\text{mg m}^{-2}$ ) by assuming a constant C:Chl a ratio ( $r_{C:Chla}$ ) of 80:1 based on Wetzel et al. (27). This is a simplification of real biological processes in the ocean where  $r_{C:Chla}$  is known to vary as a function of light limitation, depth, and phytoplankton growth rates among other factors (33).

$$(6) \quad C_{OC} = C_{T-Chl} \cdot r_{C:Chla}$$

We approximate the concentration of suspended particles in each model grid cell from wet weights of planktonic biomass that are derived by assuming that organic carbon is 50% of the dry weight and the dry weight is 20% of the weight for phytoplankton, resulting in an overall conversion factor of 10 mg wet weight: mg carbon (34). This results in an overall conversion factor of 10 mg wet weight: mg carbon.

$$(7) \quad C_{SPM} = 10^3 (C_{OC} \cdot M_{wet} \cdot A_w) / z_{MLD}$$

Although the majority of particles in open ocean environments are living and dead planktonic biomass, we allow for up to an additional 10% increase in  $SPM$  to account for allochthonous abiotic particles such as mineral dust (35).

**Table S3.** Model representation of redox reactions.

$k_{ox1}$ ( $s^{-1}$ )	Photo-oxidation rate constant	$6.6 \times 10^{-6} \cdot R$ (25) When $R > 0$ <i>min</i> : $5.6 \times 10^{-6} s^{-1}$ (36) <i>max</i> : $9.7 \times 10^{-4} s^{-1}$ (25)
$k_{ox2}$ ( $s^{-1}$ )	Dark oxidation rate constant	$1.0 \times 10^{-7}$ (36, 37)
$k_{red1}$ ( $s^{-1}$ )	Photolytic reduction rate constant	$1.7 \times 10^{-6} \cdot R$ (25) When $R > 0$ <i>min</i> : $< 1.0 \times 10^{-7} s^{-1}$ (25, 36) <i>max</i> : $8.7 \times 10^{-4} s^{-1}$ (25)
$k_{red2}$ ( $s^{-1}$ )	Biotic reduction rate constant	$4.5 \times 10^{-6} \cdot NPP$ (25) <i>min</i> : $3.5 \times 10^{-7} s^{-1}$ <i>max</i> : $8.3 \times 10^{-5} s^{-1}$ (38)
$R$ ( $W m^{-2}$ )	Average shortwave radiation intensity in the mixed layer	$\int_0^{MLD} R_i$
$\int_0^{MLD} R_i$ ( $W m^{-2}$ )	Total local shortwave radiation penetration in the mixed layer	$\frac{1}{x_2 - x_1} \cdot \frac{R_i}{\eta} [e^{\eta x_1} - e^{-\eta x_2}]$
$R_i$ ( $W m^{-2}$ )	Total shortwave radiation intensity	GEOS-5 meteorology
$x_1$ (m)	Surface depth	0 m
$x_2$ (m)	Bottom depth	$z_{MLD}$
$\eta$ ( $m^{-1}$ )	Extinction coefficient for radiation	$\eta_w + \eta_{chl} C_{chl} + \eta_{DOC} C_{DOC}$
$\eta_w$ ( $m^{-1}$ )	Extinction coefficient for water	450 nm (vis) = 0.0145
$\eta_{Chla}$ ( $m^{-1}$ )	Extinction coefficient for pigments	450 nm (vis) = 31
$C_{Chla}$ ( $mg L^{-1}$ )	Average concentration of Chl a in mixed layer	$(C_{T-Chl} \cdot A_w) / z_{MLD}$
$\eta_{DOC}$ ( $mg L^{-1}$ )	Extinction coefficient for dissolved organic carbon (DOC)	450 nm (vis) = 0.654
$C_{DOC}$ ( $mg L^{-1}$ )	Concentration of DOC in water column	$1.5 \cdot (NPP / NPP_x)$ (39)
$NPP$ ( $gC m^{-2} d^{-1}$ )	NPP in model grid cell	2003 MODIS satellite data (28)
$NPP_x$	Global average NPP	global NPP/ocean surface area

**Table S4.** Gas exchange parameterization.

$M_{ev}$ (kg s <sup>-1</sup> )	Air-sea exchange of Hg <sup>0</sup> for each model time step ( $dt$ )	$(10^{-12} F_v \cdot A_w) dt / 3600$
$F_v$ (ng m <sup>-2</sup> h <sup>-1</sup> )	Hg <sup>0</sup> air-sea exchange flux	$F_v = K_w (C_w - C_a / H'(T))$
$C_{wHg^0}$ (ng m <sup>-3</sup> )	Concentration of Hg <sup>0</sup> in seawater	See differential equations
$C_{aHg^0}$ (ng m <sup>-3</sup> )	Concentration of Hg <sup>0</sup> in air	GEOS-Chem atmospheric simulation
$H'(T)$	Temperature dependent dimensionless Henry's law constant	$\ln H' = \left( \frac{-2403.3}{T} + 6.92 \right) (40)$
$K_w$ (m hr <sup>-1</sup> )	Water-side mass transfer coefficient for steady winds	$A \times u_{10}^2 (Sc / Sc_{CO_2})^{-0.5} (41)$
$A$ (unitless)	Constant based on the Weibull distribution of wind speeds over oceans	0.25 (6)
$u_{10}$ (m s <sup>-1</sup> )	Wind speed normalized to 10 m above sea surface	GEOS-5 data
$Sc_{CO_2}$	Schmidt number for CO <sub>2</sub>	$0.11T'^2 - 6.16T' + 644.7 (42)$
$T'$ (°C)	Water temperature	GEOS-5
$Sc_{Hg(0)}$	Schmidt number for Hg(0)	$\nu / D$
$\nu$ (cm <sup>2</sup> s <sup>-1</sup> )	Kinematic viscosity	$N/\rho = 0.017e^{(-0.025T')} (42)$
$N$ (cP)	Viscosity of water	See text
$\rho$ (mg cm <sup>-3</sup> )	Seawater density	
$D$ (cm <sup>2</sup> s <sup>-1</sup> )	Diffusivity (Wilke-Chang (3) method)	$\frac{7.4 \times 10^{-8} (\phi_w M_w)^{1/2} T}{NV_B^{0.6}}$
$M_w$ (g mol <sup>-1</sup> )	Molecular weight of water	18.0
$T$ (K)	Water temperature in Kelvin	GEOS-5 data
$V_B$ (cm <sup>3</sup> mol <sup>-1</sup> )	Molal volume of mercury at its normal boiling temperature	12.74
$\phi_w$	Solvent association factor introduced to define the effective molecular weight of the solvent with respect to the diffusion process	2.26 (43)

### Aqueous Viscosity

Loux (44) provides the following relationship for estimating aqueous viscosity as a function of aqueous temperature between 0-20°C:

$$(8) \log(N) = \frac{1301}{(998.333 + 8.1855(T' - 20) + 0.00585(T' - 20)^2)} - 3.30233$$

For water temperatures 20-100°C:

$$(9) \log(N_T / N_{20}) = \frac{1.3272(20 - T') - 0.001053(T' - 20)^2}{T' + 105}$$

Where  $N_{20}$  = aqueous viscosity at 20°C.

#### Section IV: References Cited

- (1) Qureshi, A.; O'Driscoll, N. J.; MacLeod, M.; Neuhold, Y. M.; Hungerbuhler, K., Photoreactions of Mercury in Surface Ocean Water: Gross Reaction Kinetics and Possible Pathways. *Environmental Science & Technology* **2010**, *44*, (2), 644-649.
- (2) Loux, N. T., A critical assessment of elemental mercury air/water exchange parameters. *Chemical Speciation and Bioavailability* **2004**, *16*, (4), 127-138.
- (3) Wilke, C. R.; Chang, P., Correlation of diffusion coefficients in dilute solutions. *Aiche Journal* **1955**, *1*, (2), 264-270.
- (4) Kuss, J.; Holzmann, J.; Ludwig, R., An Elemental Mercury Diffusion Coefficient for Natural Waters Determined by Molecular Dynamics Simulation. *Environmental Science & Technology* **2009**, *43*, (9), 3183-3186.
- (5) Liss, P. S.; Merlivat, L., Air-sea exchange rates: Introduction and synthesis. In *The role of Air-Sea Exchange in Geochemical Cycling*, Buat-Menard, P., Ed. D Reidel Publishing Compant: Dordrecht, 1986; pp 113-127.
- (6) Nightingale, P.; Malin, G.; Law, C.; AJ, W.; Liss, P.; Liddicoat, M.; Boutin, J.; Upstill-Goddard, R., In situ evaluation of air-sea gas exchange parameterizations using novel conservative and volatile tracers. *Global Biogeochemical Cycles* **2000**, *14*, (1), 373-387.
- (7) Rolffhus, K.; Fitzgerald, W. F., The evasion and spatial/temporal distribution of mercury species in Long Island Sound, CT-NY. *Geochimica et Cosmochimica Acta* **2001**, *65*, (3), 407-418.
- (8) Sunderland, E. M.; Dalziel, J.; Heyes, A.; Branfireun, B. A.; Krabbenhoft, D. P.; Gobas, F., Response of a Macrotidal Estuary to Changes in Anthropogenic Mercury Loading between 1850 and 2000. *Environmental Science & Technology* **2010**, *44*, (5), 1698-1704.
- (9) Andersson, M. E.; Gardfeldt, K.; Wangberg, I.; Sprovieri, F.; Pirrone, N.; Lindqvist, O., Seasonal and daily variation of mercury evasion at coastal and off shore sites from the Mediterranean Sea. *Marine Chemistry* **2007**, *104*, (3-4), 214-226.
- (10) Soerensen, A.; Sunderland, E.; Holmes, C.; Jacob, D. J.; Yantosca, R.; Strode, S.; Skov, H.; Christensen, J.; Mason, R. P., A new global simulation of mercury air-sea exchange for evaluating impacts on marine boundary layer concentrations. *Environmental Science & Technology* **2010**, *submitted*.
- (11) Sunderland, E. M.; Krabbenhoft, D. P.; Moreau, J. W.; Strode, S. A.; Landing, W. M., Mercury sources, distribution, and bioavailability in the North Pacific Ocean: Insights from data and models. *Global Biogeochemical Cycles* **2009**, *23*, 14.
- (12) Laurier, F.; Mason, R.; Gill, G.; Whalin, L., Mercury distribution in the North Pacific Ocean - 20 years of observations. *Marine Chemistry* **2004**, *90*, (1-4), 3-19.
- (13) Mason, R. P.; Fitzgerald, W., Alkylmercury species in the equatorial Pacific. *Nature* **1990**, *347*, 457-459.
- (14) Mason, R. P.; Fitzgerald, W., The distribution and cycling of mercury in the equatorial Pacific Ocean. *Deep-Sea Research Part I: Oceanographic Research Papers* **1993**, *40*, (9), 1897-1924.
- (15) Gill, G.; Bruland, K., Mercury in the northeast Pacific Ocean. *EOS Trans. Amer. Geophys. Union* **1987**, *68*, 1763.
- (16) Gill, G.; Fitzgerald, W. F., Vertical mercury distributions in the oceans. *Geochimica Cosmochimica Acta* **1988**, *52*, 1719-1728.
- (17) Mason, R.; Lawson, N.; Sheu, G.-R., Mercury in the Atlantic Ocean: factors controlling air-sea exchange of mercury and its distribution in upper waters. *Deep-Sea Research II* **2001**, *48*, 2829-2853.

- (18) Mason, R.; Sullivan, K. A., The distribution and speciaiton of mercury in the South and equatorial Atlantic. *Deep-Sea Research II* **1999**, *46*, 937-956.
- (19) Mason, R.; Rolffhus, K.; Fitzgerald, W., Mercury in the North Atlantic. *Marine Chemistry* **1998**, *61*, 37-53.
- (20) Kirk, J. L.; St. Louis, V.; Hintelmann, H.; Lehnherr, I.; Else, B.; Poissant, L., Methylated mercury species in marine waters of the Canadian High and Sub Arctic. *Environmental Science and Technology* **2008**, *42*, (22), 8367-8373.
- (21) Kim, J.; Fitzgerald, W., Sea-Air partitioning of mercury in the equatorial Pacific Ocean. *Science* **1986**, *231*, (4742), 1131-1133.
- (22) Kim, J.; Fitzgerald, W., Gaseous mercury profiles in the tropical Pacific Ocean. *Geophysical Research Letters* **1988**, *15*, 40-43.
- (23) Gardfeldt, K.; Sommar, J.; Ferrara, R.; Ceccarini, C.; Lanzillotta, E.; Munthe, J.; Wangberg, I.; Lindqvist, O.; Pirrone, N.; Sprovieri, F.; Pesenti, E.; Stromberg, D., Evasion of mercury from coastal and open waters of the Atlantic Ocean and the Mediterranean Sea. *Atmospheric Environment* **2003**, *Supplement No. 1*, S73-S84.
- (24) Guentzel, J. L.; Powell, R. T.; Landing, W. M.; Mason, R. P., Mercury associated with colloidal material in an estuarine and open-ocean environment. *Marine Chemistry* **1996**, *55*, 177-188.
- (25) Whalin, L.; Kim, E.; Mason, R., Factors influencing the oxidation, reduction, methylation and demethylation of mercury species in coastal waters. *Marine Chemistry* **2007**, *107*, 278-294.
- (26) Montegut, C. D.; Madec, G.; Fischer, A. S.; Lazar, A.; Iudicone, D., Mixed layer depth over the global ocean: An examination of profile data and a profile-based climatology. *Journal of Geophysical Research-Oceans* **2004**, *109*, (C12), 20.
- (27) Wetzel, P.; Maier-Reimer, E.; Botzet, M.; Jungclaus, J.; Keenlyside, N.; Latif, M., Effects of ocean biology on the penetrative radiation in a coupled climate model. *Journal of Climate* **2006**, *19*, (16), 3973-3987.
- (28) Behrenfeld, M. J.; Falkowski, P. G., Photosynthetic rates derived from satellite-based chlorophyll concentration. *Limnology and Oceanography* **1997**, *42*, (1), 1-20.
- (29) Antia, A.; Koeve, W.; Fischer, G.; Blanz, T.; Schulz-Bull, D.; Scholten, J.; Neuer, S.; Kremling, K.; Kuss, J.; Peinert, R.; Hebbeln, D.; Bathmann, U.; Conte, M.; Fehner, U.; Zeitzschel, B., Basin-wide particulate organic carbon flux in the Atlantic Ocean: Regional export patterns and potential for CO<sub>2</sub> sequestration. *Global Biogeochemical Cycles* **2001**, *15*, (4), 845-862.
- (30) Morel, A.; Berthon, J. F., Surface pigments, algal biomass profiles, and potential production of the euphotic layer - relationships reinvestigated in view of remote-sensing applications. *Limnology and Oceanography* **1989**, *34*, (8), 1545-1562.
- (31) Uitz, J.; Claustre, H.; Morel, A.; Hooker, S. B., Vertical distribution of phytoplankton communities in open ocean: An assessment based on surface chlorophyll. *Journal of Geophysical Research-Oceans* **2006**, *111*, (C8), 23.
- (32) Morel, A.; Maritorena, S., Bio-optical properties of oceanic waters: A reappraisal. *Journal of Geophysical Research-Oceans* **2001**, *106*, (C4), 7163-7180.
- (33) Westberry, T.; Behrenfeld, M.; Siegel, D.; Boss, E., Carbon-based primary productivity modeling with vertically resolved photoacclimation. *Global Biogeochemical Cycles* **2008**, *22*, GB2024.
- (34) O'Reilly, J.; Evans-Zetlin, C.; Busch, D., Primary Production. In *Georges Bank*, Backus, R. H.; Bourne, D. W., Eds. MIT Press: Cambridge, MA, 1987; pp 220-233.
- (35) Millero, F. J., *Chemical Oceanography*, 3rd ed. CRC Press: Boca Raton, FL USA, 2006; p 496.

- (36) Lalonde, J. D.; Amyot, M.; Orvoine, J.; Morel, F. M. M.; Auclair, J. C.; Ariya, P. A., Photoinduced oxidation of Hg<sup>0</sup> (aq) in the waters from the St. Lawrence estuary. *Environmental Science & Technology* **2004**, *38*, (2), 508-514.
- (37) Lalonde, J.; Amyot, M.; Kraepiel, A.; Morel, F., Photooxidation of Hg(0) in artificial and natural waters. *Environmental Science and Technology* **2001**, *35*, 1367-1372.
- (38) Amyot, M.; Gill, G. A.; Morel, F. M. M., Production and loss of dissolved gaseous mercury in coastal seawater. *Environmental Science & Technology* **1997**, *31*, (12), 3606-3611.
- (39) Chester, R., *Marine Geochemistry, 2nd Ed.* Blackwell Science Ltd.: Berlin, Germany, 2003; p 506.
- (40) Andersson, M. E.; Gardfeldt, K.; Wangberg, I.; Stromberg, D., Determination of Henry's law constant for elemental mercury. *Chemosphere* **2008**, *73*, (4), 587-592.
- (41) Wanninkhof, R., Relationship between wind-speed and gas-exchange over the ocean. *Journal of Geophysical Research-Oceans* **1992**, *97*, (C5), 7373-7382.
- (42) Poissant, L.; Amyot, M.; Pilote, M.; Lean, D., Mercury water-air exchange over the upper St. Lawrence River and Lake Ontario. *Environmental Science and Technology* **2000**, *2000*, (34), 3069-3078.
- (43) Hayduk, W.; Laudie, H., Prediction of diffusion-coefficients for nonelectrolytes in dilute aqueous solutions. *Aiche Journal* **1974**, *20*, (3), 611-615.
- (44) Loux, N. T. In *Monitoring cyclical air/water elemental mercury exchange*, 2001; Royal Soc Chemistry: 2001; pp 43-48.